Rules for the
2009 Human Powered Vehicle Challenge West
Sponsored by ASME and Portland State University

Appendix 5: Vehicle Description
Due March 20, 2009

(Dimensions in inches, pounds)

Competition Location: Portland, OR

School name: Rose-Hulman Institute of Technology

Vehicle name: Mark IV

Vehicle number 1

Vehicle type Single X Multi-rider _____ Utility _____

Vehicle configuration

Upright _____ Semi-recumbent X

Prone _____ Other (specify) _____

Frame material Carbon fiber, Kevlar fiber, steel

Fairing material(s) Carbon fiber, Kevlar fiber

Number of wheels 2

Vehicle Dimensions

Length 96 in Width 21 in

Height 38 in Wheelbase 49.2 in

Weight Distribution Front 55% Rear 45% Total 100%

Wheel Size Front ISO 406x28 Rear ISO 406x44

Frontal area 524 in^2

Steering Front X Rear _____

Braking Front _____ Rear _____ Both X

Estimated Cd 0.084

Vehicle history (e.g., has it competed before? where? when?)

The vehicle prototype has not competed. All riders have ridden the vehicle prototype for a combined total of 10 hours.

Rose-Hulman Institute of Technology

2009 ASME West Coast HPV Competition

Single Rider Entry Team 1

Team Members

Danny Sing
Molly Nelis
Chris Wlezien
Ariel Young
Jeffery Van Treuren

Rachelle Cobb
Sean Hannon
Jeffery Dovalovsky
Cole Pearson
Andrew Bomar

Contents

Abstract

The Rose-Hulman Human Powered Vehicle Team has researched, developed, fabricated, and raced short wheelbase, low racer recumbent bicycles for four years. In 2008, the Infinity, Figure 1, took 1st place at the East and West Coast HPV Challenges. The 2009 vehicle, Mark IV, will be a higher, wider, and lighter vehicle specifically designed to be more stable, have better handling, and have a more compact drive train than the Infinity.

Figure 1: Evolution of Design
(Left) 2007 R5 (Middle) 2008 Infinity (Right) 2009 Mark IV

Using experience accumulated over the past four years, we have identified the strengths and weaknesses in previous designs. For strengths, we have determined that a tub frame is the best way to protect our riders during crashes. The strongest, most rigid part of our vehicle, the fairing, separates the rider from the road surface and objects with which the vehicle may collide. A head bubble allows for a more upright seat position and a steeper windshield, which enhances control of the vehicle and improves forward stability.

Stability and control have been identified as weaknesses in previous designs. This year we performed extensive calculations on steering geometry to improve stability and handling. By making a larger fairing, we have allowed riders more room for better control of the bicycle. Despite having a larger fairing, extensive analysis of fairing shapes has improved the aerodynamic properties of our vehicle. Previous drive trains have resulted in rider clearance issues. The Mark IV drive train will have a narrower spindle and narrower cranks, also known as a narrow Q-factor. Another weakness in previous designs has been excessive weight. This year, to reduce weight, we have made more efficient use of material in the fairing through ribbing. Thick ribs will be used to provide structural support in key areas, and a strong, but light, composite skin will cover the outside of the fairing. More weight-efficient methods of attaching the steel frame to the fairing will also be implemented.

Mission Statement 2008-2009:
Design, Test, Build and Race the Mark IV, a safe vehicle with improved endurance performance and a top speed exceeding 45mph in competition.

Figure 2: Prototype

1 Design and Innovation

This section covers the design of the vehicle and begins by defining vehicle goals. The most important vehicle features were identified using a Quality Function Deployment (QFD). An outline of research into prior art and innovative design features follows.

1.1 Team Goals

At the beginning of the year, our team laid out a list of goals we would like to achieve with the Mark IV design.

Table 1: 2009 Vehicle Goals

Team Goals	• >45mph HPVC Sprint Speed • Improved seat angle • Decreased weight • Enhanced stability

1.2 Constraints

Throughout the design process it was necessary to ensure that the vehicle was within certain constraints. Most of these constraints were imposed by the safety rules of the 2009 HPVC. Additional constraints were based on Human Powered Race Association safety rules, the Rose-Hulman team's own consideration for safety, and the necessities of transporting the vehicle. Below, Table 2 outlines these constraints.

Table 2: 2009 Vehicle Constraints

Constraints	• 15 ft. turn radius • Braking from 15 to 0 mph in < 20ft. • Independent and redundant braking system • Capable of traveling >100 ft. in straight line • Roll bar passing 600 lb_f top load with elastic deflection less than 2" • Roll bar passing 300 lb_f side load with elastic deflection less than 1.5" • Safety harness (seatbelt) ≥ 3 points • Rider protection from sliding/abrasion • Mirrors demonstrating rear visibility to both sides • No exposed carbon on the vehicle interior • Less than 8 feet long

1.3 Quality Function Deployment

The team brainstormed the strengths and weaknesses of the 2008 Infinity, to assist in the development of the QFD. The results point to visibility, stability, and weight as areas for improvement this year.

Table 3: Brainstorming Improvements on 2008 Vehicle

Strengths	Weaknesses	Improvements
Monocoque fairing	Weight	Lighter fairing
Crashworthiness	Time to change wheels	Rear visibility
Narrow Q-factor	Tiller steering	Steering stability
Protected derailleur	Visibility	

After brainstorming the list of improvements, our team employed a QFD tool in order to identify the most important issues associated with the human powered vehicle design. The QFD uses the customer and design requirements to determine the relative importance of each design criteria. The highlighted row of the QFD shows the relative importance of each of our defined design requirements. Figure 3 details the QFD done for this year's human powered vehicle at the ASME HPVC.

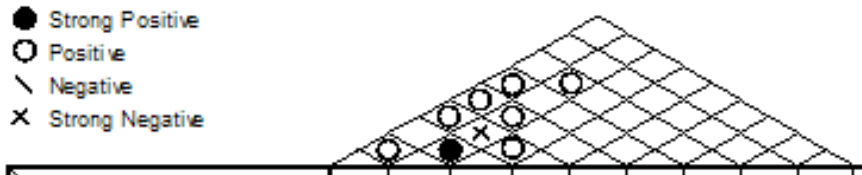

Customer Requirements (WHATs) \ Design Requirements (HOWs)	Vehicle Height	Weight	Number of Wheels	Cost	Max Rider Height	Seatback Angle	Crank Length	Field of View	Turn Radius	Customer Importance	Current Competition	Planned Vehicle	Improvement Ratio	Sales Points	Absolute Improvement	Relative Improvement
Fast	9		9	1	9	9	3	1	1	5	4	5	1.25	2	12.5	0.20
Stable	9		3			9	1	3	9	5	5	5	1.00	2	10.0	0.16
Safe		1	1	3				9	1	5	4	5	1.25	2	12.5	0.20
Durable		1		1						4	2	3	1.50	1	6.0	0.10
Time to Deliver		1	1	1						3	4	4	1.00	1	3.0	0.05
Lightweight Vehicle	1	9	3	9	1					4	5	5	1.00	2	8.0	0.13
Repairable		3		1				1		2	3	3	1.00	1	2.0	0.03
Low Cost		9	3	9	1					1	3	2	0.67	1	0.7	0.01
Innovative		3		1						3	3	4	1.33	2	8.0	0.13
Maneuverable	1	1	1			3		9	3	3	5	5	1.00	2	6.0	0.10
Abs. Importance	3.45	2.16	3.03	2.35	1.93	3.52	0.76	3.37	2.12	23					68.7	1.00
Rel. Importance	0.15	0.10	0.13	0.10	0.09	0.16	0.03	0.15	0.09	1.00						
Current Competition	38	65	2	10	6	41	155	170	15							
Improvement Direction	▲	▼	o	▼	▲	▲	o	▲	o							
target value	40	60	2	7	6.1	42	155	300	15							
units	in	lb	unit	1k$	ft	deg	mm	deg	ft							

Figure 3: House of Quality

The result of this exercise was an increased understanding on the value associated with each of the design characteristics. From the relative importance line, you can see that important aspects of the design are vehicle height, seatback angle, the number of wheels, cost, and weight. The house of quality has shown that we should concentrate on the areas of seatback angle, weight, and field of view from the design requirements as well as speed, stability and safety, from the customer requirements.

1.4 Research and Innovation

Based on the goals and constraints for the year, our QFD, and the areas in which our knowledge was more limited, the team chose to focus its research in the areas of weight reduction, steering, and aerodynamics. Ribbed construction was researched to reduce weight. A remote tiller system and two-wheel steer were explored to improve steering, and a narrower hub and improved seaming were also examined for aerodynamic improvements. Additional research was performed on automatic transmissions, cost, and abrasion resistance.

1.4.1 Ribs

The design of the 2008 Infinity, with respect to the continuous core, resulted in an extremely stiff and strong monocoque frame. The down side was that, due to inexperience and manufacturing difficulties, the Nomex honeycomb in the bottom of the vehicle was mostly filled with resin. This resulted in a much heavier vehicle than necessary. To avoid reoccurrence, we have reduced the area that the Nomex covers, while increasing the thickness in some regions. The ribs will provide all of the strength necessary, while the skin between the ribs acts as a shear web like an aircraft wing. These ribs would be laid out like the hull of a boat. There will be a double keel and three perpendicular ribs made of ¾" thick Nomex [1]. The gunwale, or top rim, is made of ¼" thick Nomex, as seen in Figure 4.

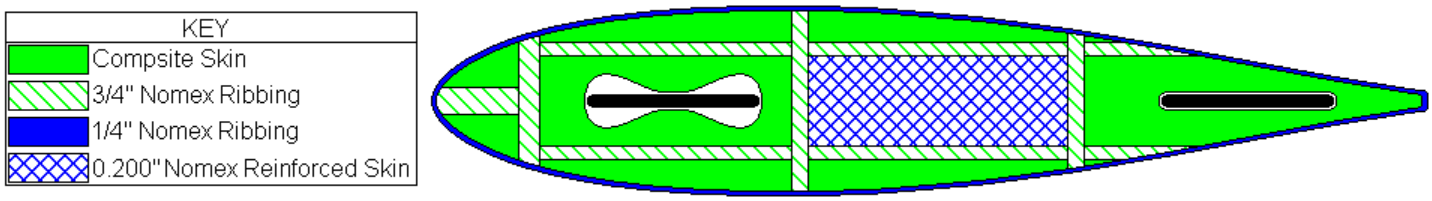

Figure 4: Bottom Fairing Rib Layout

1.4.2 Remote Tiller Steering

The Mark IV will be equipped with an improved tiller-based steering system, as shown in Figure 5.

Figure 5: Remote Tiller on the Prototype

Our previous vehicles have all had traditional tiller steering systems which are narrower than horizontal handlebars but often excessively long. When the Mark IV steering geometry was calculated, the vehicle was designed to have a 20 cm tiller length. However, due to the desired wheel base, weight distribution, head tube angle, and handlebar position, the tiller would have to be twice as long in order to end in the same position relative to the rider. Our team began to explore a remote steering system to accommodate all of the desired dimensions. The tiller rotates about a second steer tube which is then connected to the steer tube on the fork via a simple four bar mechanism, which allows the tiller length to be independent of the head tube location.

1.4.3 Two-Wheel Steering

The determining factor on the width of the front of the vehicle is the riders' feet, which is determined by the space needed to clear the front wheel. The initial idea behind rear wheel steer was that turning radius can be maintained with less front wheel steering rotation allowing the front of the vehicle to be narrower, and therefore more aerodynamic. An alternative benefit we discovered to this is lowering the minimum turn speed. A cable controlled four bar linkage was devised to steer the rear wheel, and a cable controlled internally steered hub was placed on the front. Positive trail of the rear wheel was chosen for speed stability, and the lean steer error is countered by the front steering wheel avoiding the inherent lean instabilities discussed by Cornelius [2] and Whitehead [3]. By relocating the cable to handlebar interfaces, rear steering effect was tunable (see Figure 6).

Figure 6: Prototype Two Wheel Steered Vehicle

Using this tuning and altering the lengths of the four bar linkage reconfigured the rear wheel such that it experiences very little rear steering deflection per input in many front steering angles yet experiences large steering deflections per input at large steering angles. This makes the vehicle at course speeds and turn angles handle much like it would without the rear steer mechanism, at very large steering angles found only at very low speeds the vehicle is capable of turning sharply to avoid a fall due to max steering angle constraints. Because of the lateral movement of the contact patch, less lean was required at large steering angles reducing ground interference issues with the side of the tub frame.

In the final design we decided not to include rear wheel steering. Steering with the rear wheel would have required us to widen the tail of the vehicle instead of narrowing it as the pass through hub enables us to do. The need for reduced lean angles was eliminated by increasing the height of the vehicle.

1.4.4 Pass-Through Hub

Throughout the design of the Mark IV, the aerodynamic and structural teams have worked together to create a design meeting the goals of both teams. One area where this came to be an issue was the fairing around the rear wheel. The aero team wanted to narrow the rear of the vehicle as much as possible. The structural team needed sufficient room to mount and remove the rear wheel as quickly and efficiently as possible.

The structural team determined that the inside width required for the rear wheel would be the sum of the hub outer locknut dimension (100mm), two dropouts (7mm each), the quick release head and arm (open, 75mm), symmetry on the other side (75mm), and 10mm on each side for error and working space. This totals to 284mm. The aero team wanted the rear to be as narrow as possible, preferably the 100mm width of the rear hub.

In our all wheel steer experiments the rear axle was used as a structural member. Following this idea, we began researching prior art on mountain bike pass through hubs. Along this path we found the SRAM Maxle. The design team approved of the general design of the Maxle. Rather than bonding drop outs to bosses within the rear of the frame the skewer would pass directly through the frame.

Narrowing the tub frame in the tail section removed the need for boss mounted dropouts and allows access to the securing mechanism from the outside of the vehicle. However, the quick release lever would have to protrude beyond the walls of the vehicle, or have a special external compartment designed for it. As a result, a bolt in skewer was designed to sit flush with the side of the vehicle. Every member of the team on the course will be equipped with the appropriate tool to remove the axle, removing the need for a quick release lever, which would still have to be unscrewed for wheel removal. The end result of this feature is a rear end which is has internal dimensions 65% narrower and completely locates the wheel, preventing poor alignment due to installation error.

1.4.5 Fairing Seaming

The interface of the top and bottom portions of the fairing must hold a tight tolerance for a secure fit and should be simple enough to quickly load and unload a rider. Horizontal stiffening ribs of the canopy and tub frame are butted against one another to support the connection. To hold the canopy in place, the skin of the canopy will be extended, and the tub frame's skin will be built to a point respectively lower on the bottom rib. We expect that the skin overlapping the parting line will be enough to hold the canopy in place alone. To ensure that that the top fairing is properly secured, there will be velcro straps between the top and bottom stiffening ribs on the sides of the vehicle as shown in Figure 7. The straps will be accessible by the rider allowing him or her the ability to exit the vehicle without assistance if the need arrives.

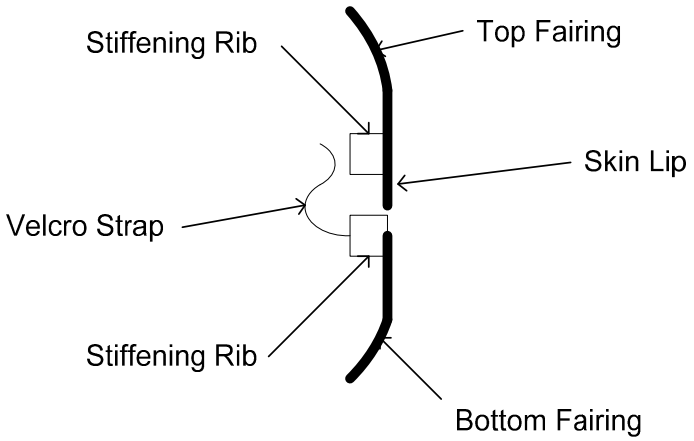

Figure 7: Top/Bottom Fairing Seam

The 2008 Infinity had tabs added to the bottom fairing as four separate pieces. It provided a two inch overlap with the top fairing and 45 square inches of contact on both sides of the vehicle. With a velcro strap holding the top fairing down, a secure fit was achieved. However, observing the Varna and CalPoly SLO's 2008 vehicle, the Athena, showed there was room for improvement in connecting the top and bottom portions of the current design. By integrating the skin overlap into the outside of the top fairing we will gain a greater contact surface area and more effective fit than adding plates on after fairing construction. To realize these gains we have moved away from monocoque construction and created a female mold with a vertical seam. After layup, the two side portions of the fairing will be seamed together permanently using the same method for installing our roll cage as explained in section 2.4. By cutting the top fairing away from the bottom fairing a proper fit will be ensured, providing greater security and faster pit times.

1.4.6 Aerodynamics

The ultimate goal for the fairing design was to create the most aerodynamic shape possible without interfering with the function of the bicycle or rider. In order to ensure that all riders would fit inside the vehicle, body measurements were taken of each rider. These measurements were used in conjunction with the specifications for the sub-frame geometry to create a fairing that would contain all possible riders.

The shape of the fairing was chosen based upon prior experience, engineering sense, and analysis with Computational Fluid Dynamics (CFD), outlined in Section 2.1. The vehicle was intended to have a minimal cross section to reduce drag, without interfering with the rider. We chose to use a head bubble design since prior vehicle design experience showed that integrated, gradually sloping windshields had poor visibility. Large integrated windshields also result in excessive temperatures inside the vehicle on hot, sunny days. We minimized length in order to maximize the vehicle's maneuverability during the endurance race and ease of transportation. To save space in the fairing, we designed the vehicle such that the rider could sit on the bottom of the fairing rather than on top of a seat.

1.4.7 Automatic Transmission

Because a majority of the riders on the team do not have extensive cycling experience, many riders have trouble maintaining an optimum pedaling cadence and are unsure exactly when to shift. There are three possible solutions to this problem. The first and simplest solution would be to increase rider training. To thoroughly train riders for maximum efficiency shifting would require more training time than our riders would be able to spare in their daily schedules. The second possible solution would be to use a device to measure the cadence of the rider. This solution would be easy to implement, as cadence sensors are commercially available. The problem is that the rider would be constantly checking the digital readout from this device which would take their concentration from the course and vehicles around them. Because of the problems associated with the first two possible solutions, a good alternative is an automatic transmission. This would allow the rider to focus on the road rather than worry about when to shift, thereby increasing the performance of our riders.

The automatic transmission uses a NuVinci Continuously Variable Planetary Hub. To control the shifting, a magnet on the wheel triggers a reed switch to convey the speed of the wheel to the microcontroller. The microcontroller then

chooses the correct gearing based the bicycle speed and a predetermined rider cadence. The microcontroller then activates a stepper motor to perform the shift. This design also allows for increased foot clearance, as there will no longer be a derailer. Due to the rapid update frequency of the transmission controller, the pedaling cadence is nearly constant. An additional benefit is that the rider will already be in the correct gear exiting a turn because the controller reads speed from the wheel rather than cadence from the crank. An override button allows the rider to temporarily increase their cadence to sprint.

One disadvantage of this solution is that the NuVinci Hub weighs approximately nine pounds as opposed to a normal derailer and cassette, which weighs approximately two pounds. Also, a battery would have to be carried to power the stepper motor and electronics, adding more weight. In the event of a failure, the system is also harder to repair than a standard drive train. It also has significantly more power losses than a standard drive train [4] so it will not be implemented on the final design.

1.4.8 Cost

The total production cost of the Mark IV is $2,396.85 which is limited to the costs of the materials used to build the vehicle. When overhead, labor, and equipment costs are factored in to the process the price increases dramatically. If great changes in the manufacturing process or design are not necessary the cost is mitigated by the projected six year production run totaling to a unit cost of $5,255.62. Our current sales model sets the customer price at $6,306.75 which will yield a total return of $756,809.84 and offsets the startup equipment cost shortly after the first month of production. See Appendix I for a list of costs.

1.4.9 Abrasion Resistance

In 2007, members tested the abrasion resistance and average skid distance for several composite samples being considered for use on the outside of a fairing [5]. Due to the Mark IV's tub frame, an abrasion resistant skin is critical for preserving the structural integrity of the entire vehicle during crashes. A skin that skids a shorter distance will make the vehicle less likely to strike other vehicles, spectators, or fixed objects during a fall.

Samples were loaded with 0.56 pounds per square inch of surface area, released onto asphalt at a speed of 30 mph, and allowed to freely slide to a stop in three separate trials. The load pressure is an estimate of what the fairing would experience if the vehicle were to slide on its side, and the speed is a conservative crash speed. The sample that was qualitatively determined to be the most abrasion resistant was a carbon-Kevlar hybrid cloth laid up so the Kevlar ran perpendicular to the velocity of the sample. Pure Kevlar also displayed great wear resistance, but had the longest average skid distance at 80 feet. The average skid distance for the hybrid cloth was 74 feet, with the shortest average skid distance among the samples tested being 55 feet [5]. Results from the skid test have led the team to select the hybrid cloth for the skin of the fairing.

2 Analysis

FloWorks, SolidWorks, ANSYS Finite Element Analysis (FEA), and by-hand methods were used to gain an understanding of how certain systems of our vehicle will behave without building physical test specimens.

2.1 Aerodynamic Analysis

To design the fairing to be as aerodynamic as possible, the fairing was designed using SolidWorks, and each design created was sent through a computational fluid dynamics simulation using COSMOS FloWorks. The models were tested at our goal speed of 20 m/s, approximately 45 mph, with a skin roughness of 250 μm. Each fairing was tested using a plane of symmetry in order to decrease the computation time, as the CAD models are designed to be symmetrical. FloWorks output a value for the drag force for each test which we then used to calculate a C_dA for comparison. After examining the results, new models were created to improve upon past versions to lower the aerodynamic drag.

Table 4 below details some of the models tested. The initial model was the design created based upon the decisions outlined in Aerodynamic Design, Section 1.4.6. Another model was tested to explore the idea of adding additional material to the sides to allow for a greater degree of movement of the rider's elbows. This idea was eventually abandoned because the increased elbow room was deemed to be not worth the aerodynamic sacrifice. In order to achieve the lowest possible C_dA while maintaining our design goals, we narrowed the rear width, lowered the nose, and tweaked the shape of certain regions. Using the final drag force values as calculated by FloWorks, we calculated the C_dA using Table 4 below.

$$Force = C_d A \frac{1}{2} \rho v^2 \quad (1)$$

Table 4: Calculated Drag Forces

Model	Drag Force (N)	C_dA (m^2)
Initial Model	6.9630	0.0290
Final Model	6.8345	0.0285
Elbow Bulges	7.1364	0.0297
2008 Infinity	7.0260	0.0293

The final model has a theoretical C_dA value of 0.0289 m^2. As stated earlier, the goal for this year's aerodynamic design was to maintain or improve upon last year's C_dA while also improving the interior space of the vehicle to allow for more clearance for rider movement. To evaluate whether or not we reached this goal, we reexamined last year's vehicle, the Infinity, testing it at the same conditions as the current vehicle, and found a C_dA of 0.0296 m^2. Therefore, we decreased our theoretical C_dA by 0.009 m^2, while increasing the clearance for rider's knees and feet compared to the team's previous vehicle.

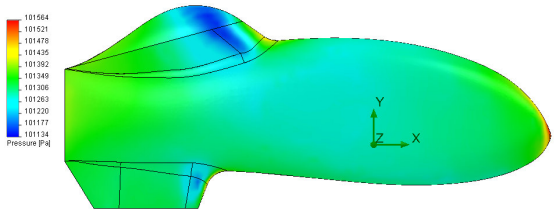

Figure 8: Final Fairing Design, Pressure Surface Plot

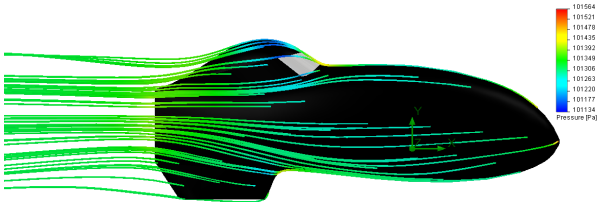

Figure 9: Final Fairing Design, Flow Trajectories

2.2 Stability Analysis

The bicycle handling characteristics are significant contributors in performance. This is especially true when the athlete is does not have years of experience with the bicycle. Traditional diamond framed upright bicycles benefit from more than a century of common use to tune handling characteristics. Recumbents vary much more in frame geometry and have not seen the same degree of refinement which safety bicycles have. As a result the general guidelines which aid designers in road bike development do not exist. One development is the text of *Lords of the Chain Ring* by Dr. Patterson of CalPoly SLO [6]. His work on single track vehicles' straight line steering response is an excellent starting point. Unlike rider perception surveys, it yields hard numbers which compares bicycles without rider experience bias on a particular vehicle. Using past experience we proposed a design for the Mark IV. Using *Lords* we plotted roll sensitivity, Figure 12, linear control sensitivity, Figure 11, roll sensitivity, Figure 12, and handlebar spring rate, Figure 10. This resulted in a complete redesign of our steering geometry. We raised the center of gravity, significantly steepened the head tube angle, and increased the offset to correct trail.

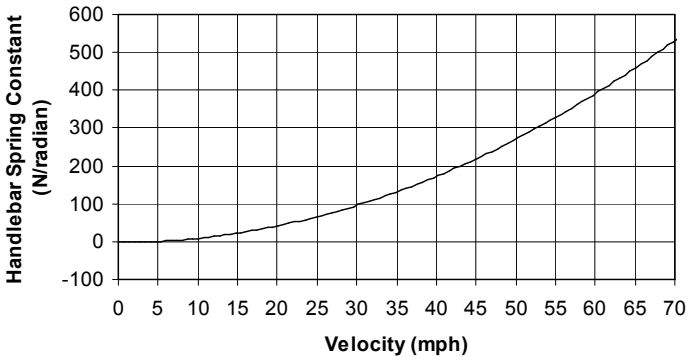

Figure 10: Steering Spring Rate Corrected for Handlebar Length (Stable Up)

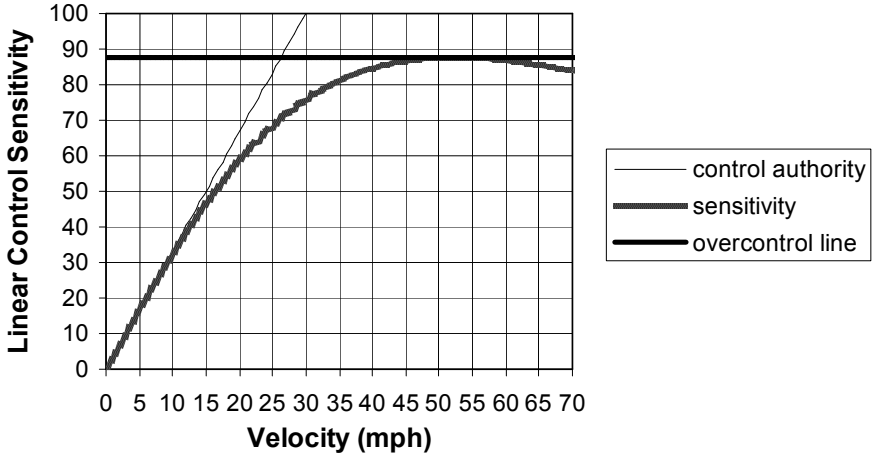

Figure 11: Linear Control Sensitivity

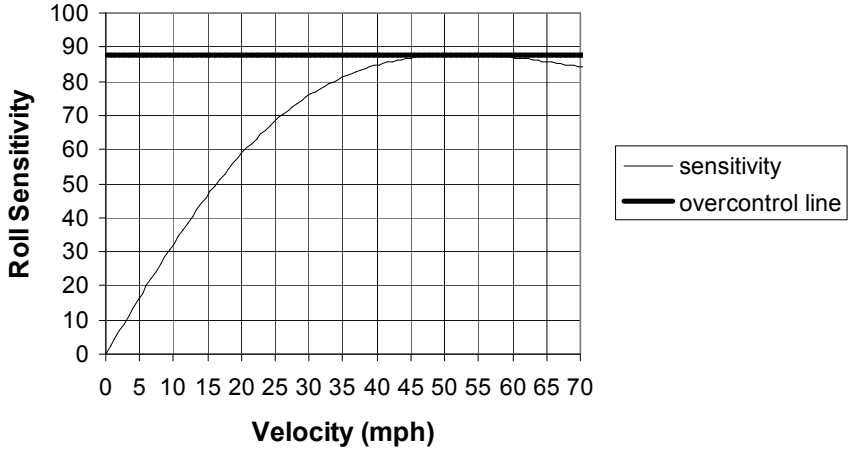

Figure 12: Roll Sensitivity (Stable Up)

The Patterson model however does not take into account geometric changes during turning such as trail changes due to handle bar turns, leanings, and front and rear wheel path differences are not considered. Y. Le Henaff discusses turns in his models [7] as does Jim Papadopoulos in his response [8]. However, these models have less useful output than the Patterson model. We have derived Dr. Patterson's formulae while taking these geometric considerations into account.

In the past straight line linear approximations of handling characteristics have been done. These studies assumed trail to be a constant value irrelevant to steering turns and bicycle leans. This model expands upon that through the use of a more complex model of trail. This model takes into account the handlebar turn and bicycle lean. Traditionally trail has been defined as[9,10]:

$$T = \frac{r \cdot \sin(\beta) - \Omega}{\cos(\beta)} \tag{2}$$

where r is the radius of the steering wheel, β is the head tube angle measured from vertical when the bicycle is not leaned, and Ω is the fork offset. In order to work with higher speeds and sharper turns lean and steering rotation must be taken into account. The resulting formula is:

$$T = \frac{r \cdot (\sin(\beta)\cos(\delta) - \tan(\phi)\sin(\delta))}{\cos(\beta)} - \Omega\sqrt{1 + \frac{(\sin(\beta)\cos(\delta) - \tan(\phi)\sin(\delta))^2}{\cos^2(\beta)}} \tag{3}$$

where ϕ is the lean angle of the frame and δ is the steering rotation angle about the head tube axis.

The direct application of this is the ability to make vehicles easier to turn without being harder to keep straight by altering wheel size and maintaining a constant trail and head tube angle. With a traditional analysis using the basic trail model in Equation (2) a compromise must be made. Generally speaking, more trail causes more stable straight line handling, but decreased turning ability. Less positive or more negative trail is more agile in turns but requires more effort in a straight line. More accurately, as lean angle increases trail decreases resulting in easier turning. In an ideal situation a bicycle would react such that when ϕ=0 trail is large helping the rider hold a steady path. When the rider turns, and accordingly leans the vehicle, trail decreases thereby increasing response frequency making turning easier. Ideally this causes the steering moment to place the wheel at an appropriate turn angle (δ). Too much negative trail and the turn is difficult to stop. This resulted in staying with an ISO 406 mm wheel rather than increasing wheel diameter. The rear rim is an ISO 406 mm to fit a Michelin Ecorun tire. The front tire, a Schwalbe Durano, is available in multiple sizes. The Mark IV has space for an ISO 520 mm rim which would decrease rolling loss. However, equation (3) shows that $\frac{\partial T}{\partial f(\delta,\phi)} \propto r$ which causes undesirable over control in our case. Weighing this decrease in handling quality with an unquantified decrease in rolling resistance, we chose the ISO 406 mm size.

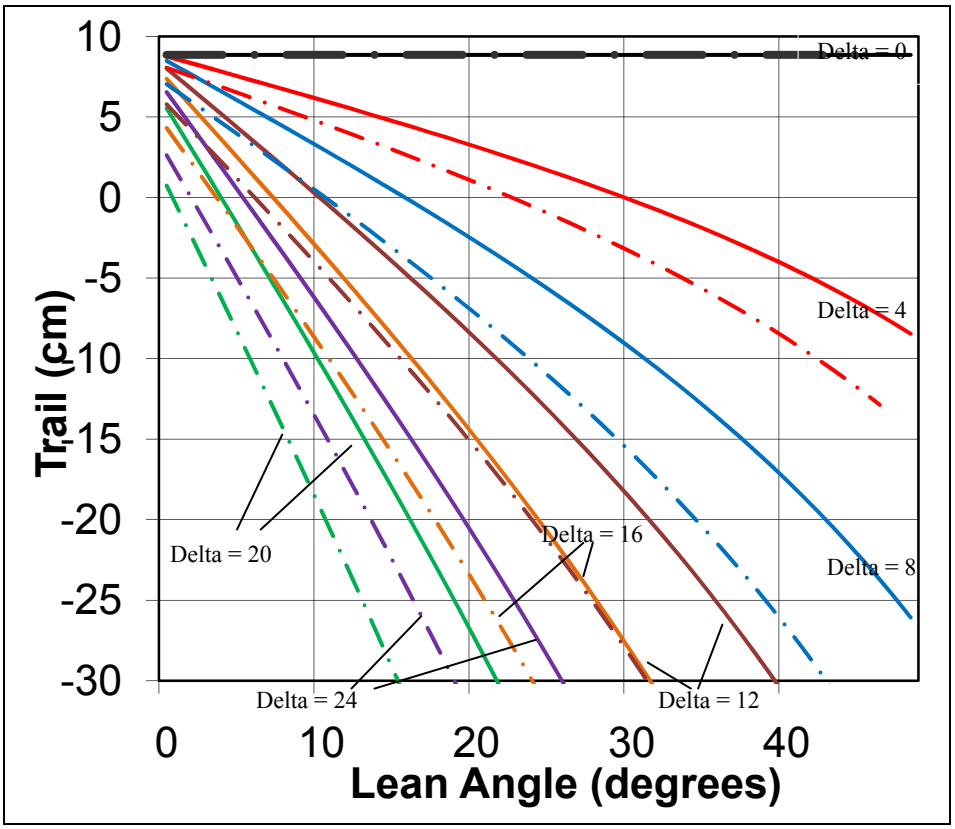

Figure 13: Trail Dependency on Lean and Turn

2.3 Rear Axle Analysis

One of this year's space and weight saving innovations is the rear pass through axle. In deciding to design our own rear axle securing device we decided to perform both a hand analysis and a finite element analysis (FEA). The first step was to determine the loads the axle would need to withstand. The axle in a Shimano HB-6600 front hub was analyzed to determine what radial point force on the wheel would be required to yield the axle. This load was then applied through hand calculations to a model of a hollow aluminum tube to determine the required tube wall thickness. The aluminum axle requires a 15 mm outer diameter axle, which is approximately 6 mm larger than a standard axle (see Table 5). The load carried by a standard axle was calculated by hand and used to find the inner diameter of the aluminum axle. The free body diagrams of the two axles depict the force of the rider through the drop out as F_L and the force opposing force as F_R (see Figure 14).

Table 5: Comparison of Axle Dimensions and Properties

	Yield Strength	Shear Strength	OD	ID	Offset
Standard Axle (chromoly steel)	400 GPa	200 GPa	8.64 mm	5.1 mm	13 mm
Pass Through Axle (6061-T6 Aluminum)	270 GPa	135 GPa	15 mm	unknown	0 mm

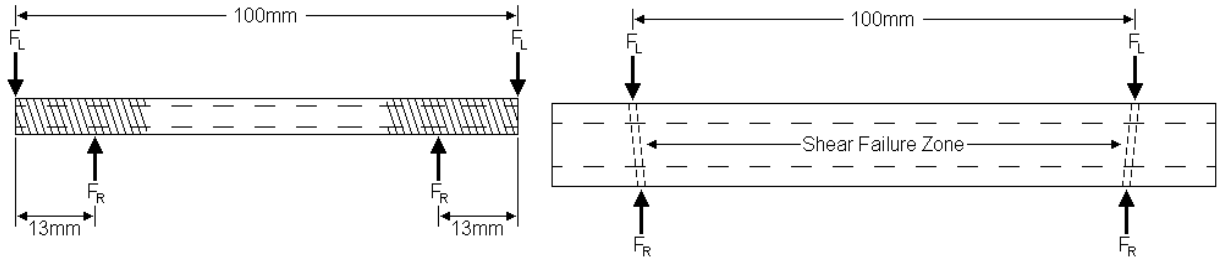

Figure 14: FBD of Standard Axle (left) and FBD of Pass Through Axle (right)

The standard steel axle fails in bending at a load of 384.82 lb_f and in shear at a load of 895.98lb_f. These numbers were calculated with Equations 4, 5, and 6 [11]. The shear and moment diagrams are shown in Figure 15.

$$\tau_{max} = \frac{V_{max} * Q}{I * t} \tag{4}$$

$$\sigma_{max} = -\frac{M_{min} * y}{I} \tag{5}$$

$$Q = \bar{y} * A_x \tag{6}$$

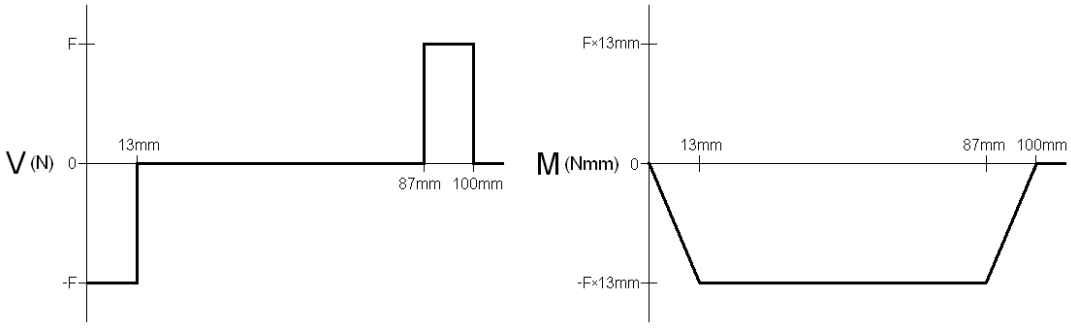

Figure 15: Shear (left) and Moment (right) Diagrams of Standard Steel Axle

The minimum aluminum axle wall thickness of 0.68mm for a factor of safety of 5 was found with Equation 7 [11].

$$\sigma_{shear} = \frac{F}{A_t} \tag{7}$$

This tube wall thickness was increased to 0.95mm to ensure a factor of safety of 7 and both increase machinability and ease concerns of crumple failure. We were unable to find an acceptable model for crumple failure of an enclosed thin walled tube in shear and as a result moved to FEA for the analysis. The original planned analysis was to be performed in the classic ANSYS interface via a script file. The drive side half of the tube was to be a 2.5 d axisymmetric model with SHELL93, and 8 node structural shell element. This would use multiple axes of symmetry to decrease the ratio of computational cost per model resolution. However, we were unable to create an acceptable model of the non-uniform bearing loading and restraints, Figure 16. As a result, the SolidWorks CAD model of the drive side half of the axle was imported into the ANSYS Workbench interface. This allowed the use of the preprogrammed bearing load, as well as the compression only support. The half model was remeshed using TET structural elements and used to determine the approximate level of mesh refinement required for a mesh independent solution. Due to the different stress concentration cases at the ends of the axle support the entire axle was modeled for the final iteration. The center had a bearing load

applied and the end sections were restrained with compression only supports. After solving the model, the strain and total deflections were checked to confirm reasonable results. Additionally, the solution was tested for mesh independence. Finally, the compression only supports were replaced with cylindrical restraints. Achieving similar results for this case, and a good convergence history, Figure 17, shows that the solution is valid due to an artifact of the boundary conditions.

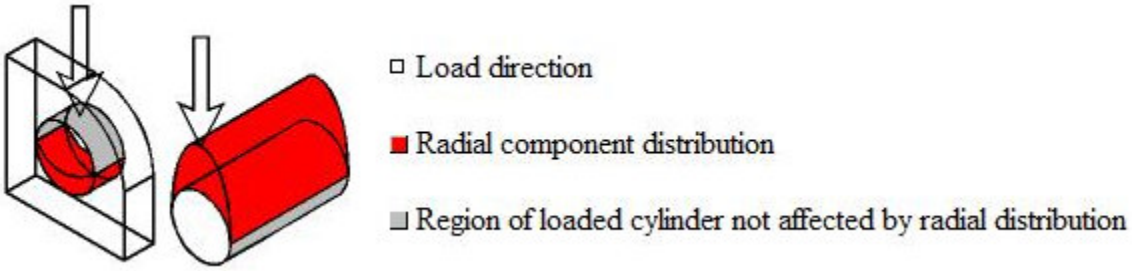

Figure 16: Bearing Load on Axle [12]

	Equivalent Stress (Pa)	Change (%)	Nodes	Elements
1	7.0464e+007		5347	2645
2	1.068e+008	40.996	23835	13479
3	1.7153e+008	46.513	72908	46248
4	2.7711e+008	47.067	120318	78926
5	2.7915e+008	0.73429	357035	246182

Figure 17: Convergence History of Final Model

The Von Mises stress was higher than the predicted average at the expected stress riser locations. The Von Mises stress, Figure 18, and shear stress were lower than the yield stress of 6061 T6 aluminum throughout the entire model by a factor of two. Additionally, the areas of peak stress are strongly localized at the edges of boundaries. Minor easing of these edges to better model the small gap between the axle and wall of the vehicle decreased the stress risers. While these changes do occur at the edges of the load and support areas they were predicted by the hand analysis and vary linearly with the magnitude of the separation. This shows that the peak stresses are not computational artifacts of the supports. Additionally, if this slight artificial rise in stress at the load and restraint interface was a computational artifact, its behavior indicates the actual part would experience less stress than the model increasing the safety factor. With this improvement the model showed a safety factor of four.

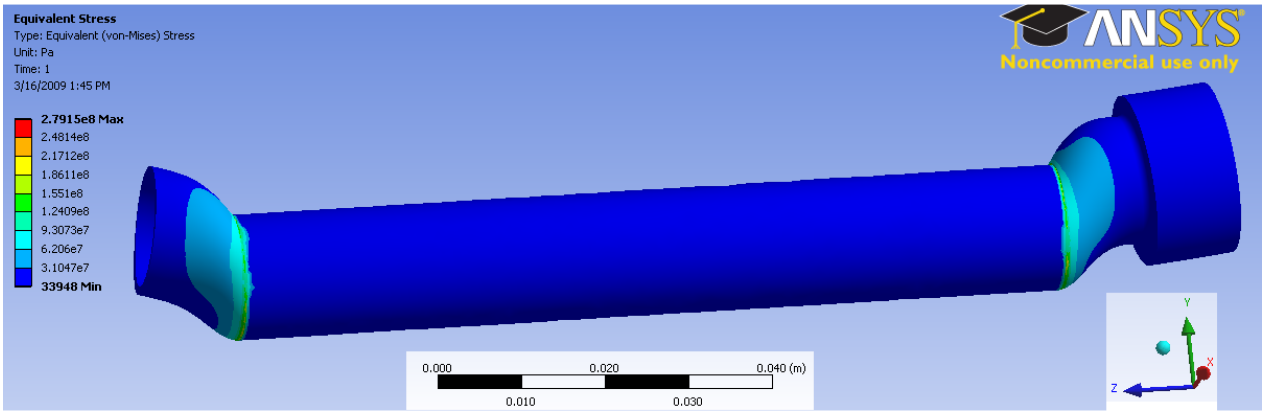

Figure 18: FEA Results

Fatigue issues were not taken into consideration given the intended lifespan of the component. The result of this analysis is confidence in the part and its design. Despite a large factor of safety, we have decided not to decrease the wall thickness of the axle. This is because the only benefits are a small weight savings and a part failure at the event could result in the withdrawal of the vehicle from competition. As a further precaution, a steel backup will be made to the same dimensions as the aluminum part.

2.4 Roll Cage Analysis

A duplicate of the roll cage was constructed in halves, using two molds, and then seamed together. The side pieces were made using the sandwich composites detailed in Figure 19. The layers of the roll cage were vacuum bagged, formed, and allowed to cure. The two sides were then aligned and attached using the seam shown in Figure 19. The layers of the seam were compressed and allowed to cure.

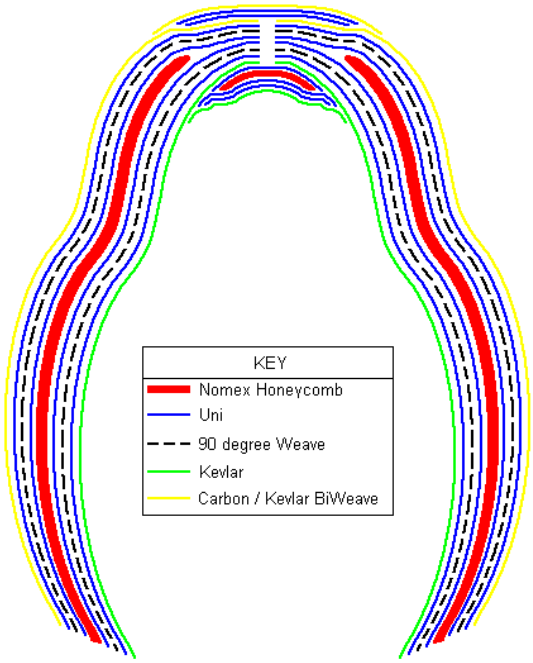

Figure 19: Roll Cage Mock Up

In order to estimate the maximum stresses that would be carried by the roll cage in each of the loading configurations, calculations were performed using Equations 8, 9, and 10, modeling the roll cage as a cantilevered beam, Figure 20. In the horizontal load case, a maximum bending stress of 10.4 ksi was found in the center of the top member. In the vertical load case, the maximum compressive stress was 3.5 ksi.

$$I = \frac{bT^3}{12} - \frac{b(T-0.21)^3}{12} \tag{8}$$

$$\sigma_{\max,bend} = \frac{FLT}{8I} \tag{9}$$

$$\sigma_{\max,comp} = \frac{F}{2b(T-0.21)} \tag{10}$$

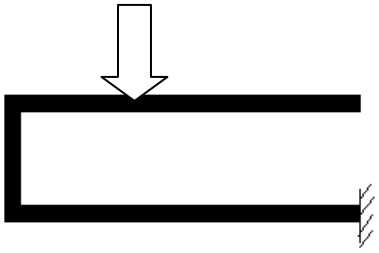

Figure 20: Roll Bar Approximation

In the horizontal load case, the roll cage was modeled as shown with the bottom member where the wheel mount is located. In this configuration the load would be applied approximately where the rider's shoulder would contact the ground. The maximum compressive stress calculated using the model was found to be 6.3 ksi. The ultimate tensile strength of the carbon fiber weave that was used in our vehicle is approximately 147 ksi, obtained from our tensile test results, which is greater than the values calculated resulting in a factor of safety of about 14.

2.5 Simple Mechanical Model

In the design of the tub frame, the stresses on the four horizontal support ribs were analyzed to determine whether the vehicle would have the necessary strength to support the forces imposed by the rider and the sub-frame. The fairing was modeled as though the weight of the rider and the vehicle were carried entirely by the four ribs on the bottom half of the vehicle, ignoring the effects of the skin. Based upon the strength of the rib samples as tested using a four-point bend test, the ribs will support the peak dynamic load of the rider and the sub-frame, with a factor of safety of 4.3, according to Equation 11.

$$W = \frac{4 \cdot \sigma_{bike}}{L_{wheelbase} \cdot y} \tag{11}$$

The maximum deflection of the rib will be 0.013 inches. This was calculated using Equation 12 and the modulus determined through the tensile testing.

$$y_{max} = -\frac{4 \cdot P \cdot \left(\frac{L_{wheelbase}}{2}\right)^3}{48 \cdot E \cdot I_{composite}} \tag{12}$$

3 Testing

Extensive testing was performed to verify analysis, ensure safety, and gain further knowledge to be used in design.

3.1 Stability Testing

Using the results of our analysis we built a prototype to test the handling and drive train. The prototype has an adjustable wheel base and fork offset for tuning purposes. Wheelbase tuning was found to be less useful, and 9 mm of offset tuning was required. The prototype is significantly more stable at low speeds than past vehicles yet is equally stable at sprint speeds. Turning is also easier. Within a week of having the prototype functioning, one member was able to make a drive train modification in front of the head tube with both hands while still pedaling and maintaining a gradual left turn on and over a short rolling hill.

In the event that the sprint course is windy and straight line stability needs to be increased, a control spring has been can be placed between the fork and the rear of the front sub frame. This will make the turning slightly more difficult but will make it easier to maintain a straight path. The spring constant required has been calculated as 10 N/rad. Knowing this in advance allows us to find a spring which meets our needs rather than having to find several springs and go through the process of empirically determining the correct spring.

3.2 Tensile Testing

The purpose of the tensile tests was to find various material properties of all of the composite materials used during the Mark IV construction. One of our main goals this year is to reduce the cost of the project overall. To do this we will the carbon that has the highest strength to cost ratio. All the carbon weaves available to us have acceptable strength to weight ratios, so cost is the driving force in determining which weight to use. It was also necessary to find our own values of Young's modulus and ultimate strength of the composite materials we were using. The tensile samples were tested in an ATS 1610 UTS machine, so the dimensions of our samples were determined from the constraints of the tester. We made two, 2" by 6" samples of each material we considered using. These samples were created with 1.5" by 2" strengthened jaw zones so the sample would not fail at the jaw (Figure 21). The samples were all three sheets of weave wide in the test zone and seven sheets wide in the jaw strengthening zone. The materials tested are tabulated below (Table 6).

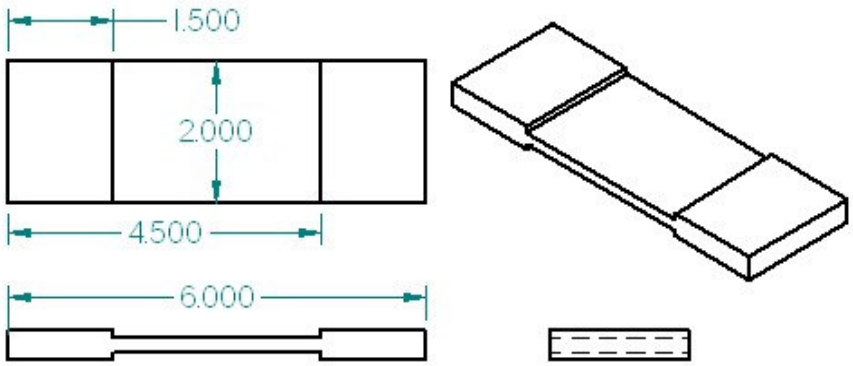

Figure 21: Standard tensile sample

Table 6: Tensile test material

Name and sample pull direction	Weight (oz/yd)	Weave	Tow (threads)	Thickness (in)
Unidirectional carbon in the carbon direction	11	Unidirectional	12k	0.021
Unidirectional carbon perpendicular to the carbon direction	11	Unidirectional	12k	0.021
Hybrid carbon and Kevlar weave in the carbon direction	5.5	2x2 twill	3K x 1500 Kevlar	0.009
Hybrid carbon and Kevlar weave in the Kevlar direction	5.5	2x2 twill	3K x 1500 Kevlar	0.009
1.7oz Kevlar in direction 90 degrees to weave	1.7	Plain	195 T1965	.004
5oz Kevlar in direction 90 degrees to weave	5	4 harness satin	1140	0.01
11oz carbon in direction 90 degrees to weave	11	2x2 twill	6k	0.017
19.7oz carbon in direction 90 degrees to weave	19.7	2x2 twill	12k	0.03
19.7oz carbon with weaves at 90, 45, and 90 degrees	19.7	2x2 twill	12k	0.03
19.7oz carbon with all weaves at 45 degrees to pull	19.7	2x2 twill	12k	0.03

All the samples were laid up with a medium epoxy room temperature cure hardener and compressed under approximately 1000 lb_f. Once they cured they were trimmed down to approximately 2" widths. The samples were all tested individually in the UTS machine. All the samples that were pulled in the direction of the weave were strained until failure and all the samples that had 45 degree sections were strained until the sample reached the ultimate stress and then strained until the stress dropped to 50% or less of that stress, or when the sample reached a percent elongation of greater than 35%.

The strength of each material relative to the others was exactly what we expected. The unidirectional carbon was pulled in the carbon directions held the most weight, followed by the 19.7 oz carbon with all the weaves at 90 degrees. The strength of the Kevlar and fiberglass were not high enough strength to cost ratios to be considered for structural purposes in the vehicle this year. The unidirectional carbon has a strength to cost ratio of 37027 psi-ft^2/$ while the 19.7 oz carbon weave has a strength to cost ratio of 14434 psi-ft^2/$. This means that, for the same amount of money, unidirectional carbon is the most cost effective material for our vehicle this year. We have decided to use the unidirectional carbon on our ribs to provide maximum strength. Since the unidirectional carbon only provides strength in one direction, we have decided to use a carbon weave as the skin material. The 11 oz carbon has a strength to cost ratio of 17319 psi-ft^2/$ which is slightly higher than the 19.7 oz carbon. However, we decided that while the strength to cost ration of the 19.7 oz carbon

is lower, it would be a better choice for the skin because it was able to take a higher force. The load to cost ratio for the 11oz carbon is lbf-ft^2/$ while it is 2063 lbf-ft^2/$ for the 19.7 oz carbon. Also, since the 19.7 oz carbon is thicker, it will provide an increased moment of inertia as compared with the 11 oz carbon without a core material. This reduces the number of lamellar needed and simplifies the construction process. So, on the basis of cost and strength, the skin material will be 19.7 oz carbon. The data from our tensile tests and cost analysis is reported below in Table 7.

Table 7: Tensile Test Data

Test Sample	Ultimate Strength (psi)	Modulus of Elasticity (psi)	Toughness (psi)	Max Load (lb_f)	Cost ($/ft^2)
Fiberglass	4.53E+04	1.08E+06	9.35E+02	2.45E+03	0.528
	4.64E+04	1.22E+06	7.73E+02	1.50E+03	
1.7 oz Kevlar	6.27E+04	1.33E+06	1.17E+03	1.06E+03	2.789
	4.95E+04	1.05E+06	9.32E+02	1.07E+03	
Unidirectional Carbon (Wrong Direction)	4.01E+03	1.39E+05	1.11E+02	3.79E+02	3.500
	4.29E+03	8.40E+04	1.02E+02	4.33E+02	
19.7 oz Carbon (90 90 90)	6.18E+04	7.66E+05	1.72E+03	7.86E+03	3.800
	4.79E+04	5.58E+05	1.71E+03	7.82E+03	
Unidirectional Carbon (Right Direction)	1.47E+05	2.32E+06	3.92E+03	1.49E+04	3.500
	1.27E+05	1.84E+06	3.78E+03	1.62E+04	
5 oz Kevlar	4.76E+04	1.15E+06	8.20E+02	2.83E+03	1.467
11 oz Carbon	5.75E+04	2.58E+05	1.39E+03	4.69E+03	3.320
Hybrid (Kevlar Direction)	2.39E+04	7.12E+05	3.38E+02	1.93E+03	2.600
	2.73E+04	4.57E+05	6.63E+02	2.02E+03	
Hybrid (Carbon Direction)	3.30E+04	5.92E+05	7.38E+02	2.30E+03	2.600
	8.79E+04	2.11E+06	1.79E+03	4.44E+03	
19.7 oz Carbon (90 45 90)	4.73E+04	6.41E+05	1.68E+03	6.89E+03	3.800
	4.28E+04	5.84E+05	1.43E+03	6.25E+03	
	3.67E+04	5.37E+02	1.52E+03	6.18E+03	
19.7 oz Carbon (45 45 45)	1.65E+04	2.07E+05	3.67E+03	2.86E+03	3.800
	1.72E+04	2.58E+05	3.43E+03	2.79E+03	

3.3 4 Point Bend Test

Once we had determined the strength of the materials, we needed to determine the effect of different core materials on the mechanical properties of the composite sandwich in order to determine the necessary materials for the structure of the vehicle. From previous testing we observed that the primary mode of failure is shear of the core [5]. We tested three methods to remedy this: resin holes, carbon channels (both with open sides), and ribbing. For the resin holes case, two samples were laid up with vinyl foam core and one of the samples had 5/16" holes drilled in an alternating one inch spacing grid. The purpose of these holes is to bond the outer skins together with resin during the laying up process. The carbon channel samples were 1/4" Nomex core except the core was not continuous; instead there were vertical sections of carbon fiber weave running lengthwise. This was done so that the spacing would be provided by the Nomex, but the shear force would be taken by the carbon channels. This is shown in Figure 22.

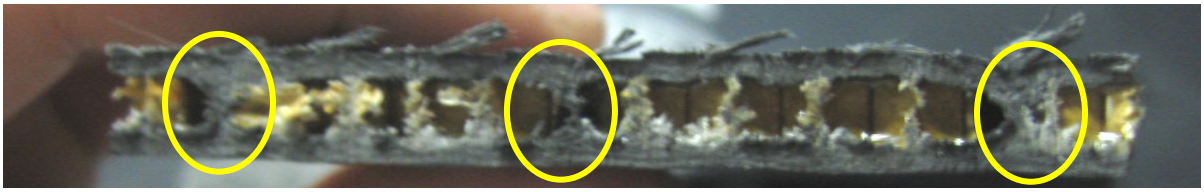

Figure 22: Carbon Channels

Lastly, the ribbing samples were constructed so that the carbon fiber covered the sides of the Nomex completely encasing the rib in carbon. The carbon along the sides of the rib would take a lot of the shear stress because of the higher modulus of elasticity while the Nomex would provide the geometry to increase the moment of inertia of the sample, Figure 23.

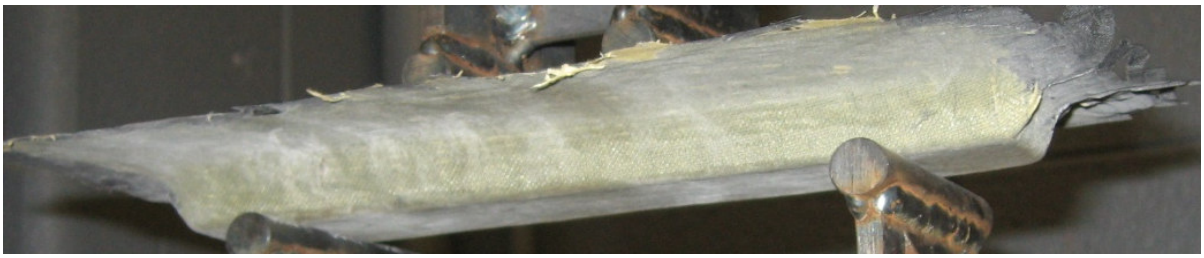

Figure 23: Ribbing

The samples and test mechanism were placed in the UTS machine to record the load and displacement of the crosshead. Each sample was tested to failure as determined by cracking of the surface lamellar or by deflection of an inch from the no load position. The data from the tensile test machine was exported to Matlab for analysis using a student written m-file.

The resin holes sample did not show significant improvement over the control. They displayed the same modulus initially with the resin holes sample being slightly stiffer. This is shown in Figure 24.

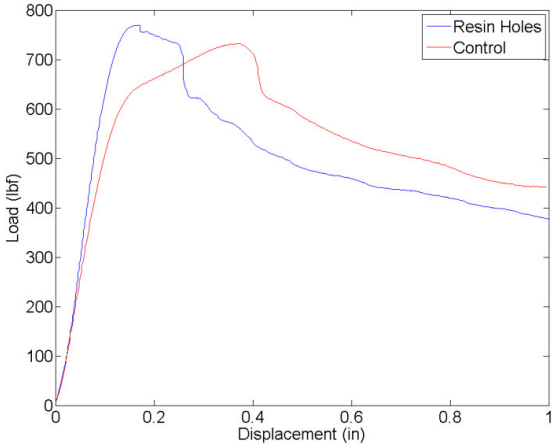

Figure 24: Resin Holes and Control

The mode of failure for the resin holes sample was the gray foam core shearing at a 45 degree angle at the location of a line of resin holes outside of the maximum moment zone. This 45 degree shear then propagated along the lower boundary connecting the core and the carbon fiber weave, Figure 25.

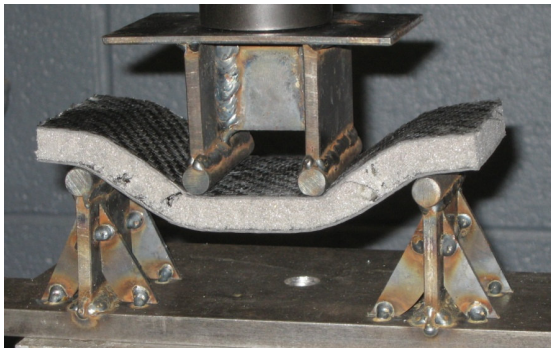

Figure 25: Resin Holes Failure

The control did not show any visible failure. The core appeared intact and completely bonded to the carbon fiber weave skin. Both samples retained a similar permanent elastic deformation even after the load was removed. The peak load carried by the resin holes sample was 769.6 lb_f and 732.6 lb_f for the control. The modulus of rupture for the resin holes and control samples were 3732.9 psi and 3535.9 psi respectively while the shear stress along the neutral axis was 298.6 psi and 282.9 psi. The slight increase in strength and stiffness of the resin holes over the control were not significant enough to ignore the increase in weight that resulted. The carbon channels on the other hand did show a marked improvement in both the stiffness and load bearing. The peak load for the carbon channels sample was 500.8 lb_f and 296.2 lb_f for the control. This is shown in Figure 26.

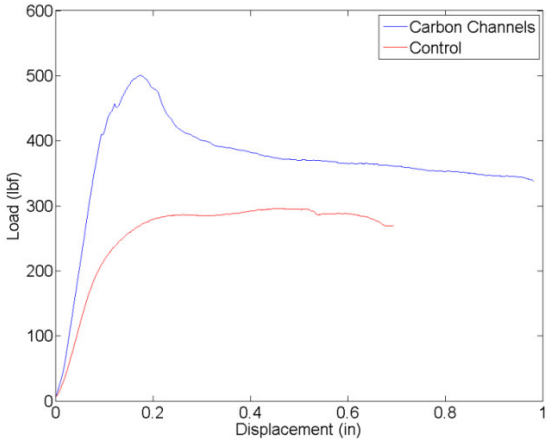

Figure 26: Carbon Channels and Control

The carbon channels sample did not visibly shear or fail in any way. It also returned to a nearly flat condition once the load had been removed. The core of the control crumpled to the extent that the two skins were in contact. After the load was removed, the core sprang back to the original shape but the sample did retain a significant plastic deformation. The maximum modulus of rupture for the carbon channels sample and the control sample were 9451.1 psi and 5694.5 psi respectively. The shear stress along the neutral axis was 384.0 psi and 229.2 psi respectively. The carbon channels sample was in all ways superior to the control; however it was far harder to lay up the carbon channels sample.

The ribs were the most successful of the 4 point bend samples. Three different thicknesses of Nomex were used for these samples: ¾”, ¼”, and 0.20 in. The 0.20 in Nomex was a higher density, 3 lb, as opposed to the 1.8 lb density for the other samples. The load-displacement data for each sample are shown in Figure 27.

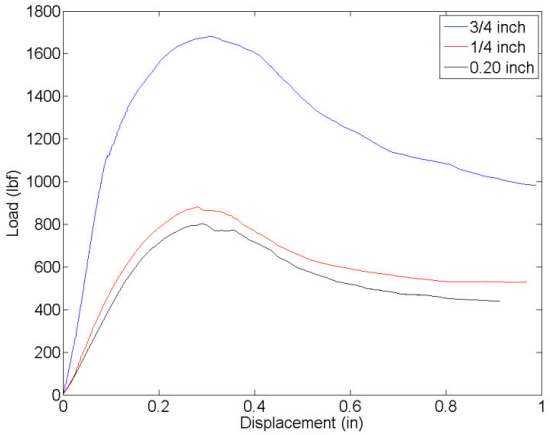

Figure 27: Ribbing

The ¾" Nomex sample held 1684.1lbf with a modulus of rupture of 8746.3 psi and a shear stress of 1057.2 psi. The ¼" sample held 881 lb_f with 2411.1 psi and 1185.0 psi stresses. The 0.20 in sample held 803.6 lb_f with 35958 psi and 1245.8 psi stresses. The reason for the increase in stress is because of the sharp decrease in the moment of inertia of the samples. The ribs were loaded a second time to determine what fraction of the peak load they could take after the catastrophic failure case from the primary loading. All samples returned to at least half of the peak from the first load by the 0.8 in displacement mark.

The results of the tests were very conclusive. The technique of ribbing can provide a great deal of strength without having to have the expensive Nomex throughout the entire vehicle. The plan is to use two ¾" thick ribs running the length of the vehicle, three ¾" ribs running up the sides of the vehicle, and a rim around the top of ¼" Nomex. These ribs will provide the structure of the vehicle and will also be the mounting points of the subframe and rear wheel. Since the rider will be sitting on the bottom of the vehicle, that area will be stiffened by a sheet of the 0.20 in Nomex. The top of the vehicle will use ¼" Nomex ribs for the support structure because, while it does need to be stiff, it does not need to support as much weight as the lower portion of the vehicle.

3.4 Roll Cage Testing

The mock roll cage was placed in a tensile test machine in a vertically with an offset of 12 degrees, as dictated in the rules. The roll bar met specifications, withstanding a compressive force of 619.2 lb_f. The deformation observed during testing was 0.830 in, with much of the compression occurring in a ¾" piece of foam used for grip, putting the deformation well within the 2 in requirement. No visual damage was observed.

In the side load configuration, the roll bar again met the requirements, sustaining a force of 386.6 lb_f without deforming significantly. We measured 0.735 in of deformation during the test; again well within the requirement of 1.5 in. No damage was heard or observed.

Finally, it was decided to reload the roll cage in the vertical position and find the point at which the roll bar would fail. However, at around 1100 lb_f, the roll bar began to slip vertically in its mounts. Despite this great load, no damage was found on the prototype roll bar.

In both load orientations the roll bar met requirements for load carrying and deformation and greatly exceeded the values dictated in the rules. The error associated with the tensile test machine used was very small, near 0.01 lb_f. Subsequent testing also showed the durability of the roll cage after various alternate loadings. To view videos and pictures of the roll cage testing please visit http://www.rose-hulman.edu/hpv/testing/2009/ASME/.

3.5 Non-Tiller Steering

To verify our steering response analysis we modified and tested a previous vehicle, the 2007 R5, to use both the remote tiller and remote horizontal handlebar steering systems. The modification of the R5 included the removal of the tiller and the creation of a new horizontal handlebar that is similar to those found on a mountain bike. After reinstalling the brake

and shifter controls the initial testing was not satisfactory. To test different hand positions we added vertical bars on the ends of the handlebar that extended above and below the horizontal handlebar.

While the horizontal handlebar did offer riders a comfortable hand position the results of our testing were not promising enough to abandon tiller steering. The primary concern is the width of the handlebar and the required distance between the arms of the rider to steer effectively. While the profile of our fairing takes into account necessary shoulder and elbow space to allow a rider to effectively navigate an endurance course, the comfortable spacing provided by the horizontal handlebar steering was excessive. There were also concerns with stability and regaining control after veering off a straight path. The bars would not allow for a rider to confidently brace themselves against pedaling forces during a sprint. The riders also would often over steer while riding this test vehicle. Based on our testing, a horizontal handlebar steering setup is not a feasible candidate for our vehicle.

3.6 Power Chair Testing

Human power output has many variables, from aerobic intake to ergonomics to thermal limits. We decided to explore the relationship between vehicle geometry and power output. We created a power chair with variable seat to bottom bracket position, in both the vertical and horizontal direction, and seat angle, measured from the horizontal plane. We intended to iterate over all three variables, however, after some research we determined that there is a professionally accepted distance from the seat to the bottom bracket for a rider [13,14]. We tested this by varying the horizontal location of the seat relative to the bottom bracket while keeping the vertical location and the seat angle fixed. Our results from that test agreed with the accepted range. NASA has performed tests similar to this. We will use this as a guideline for our testing, as seen in Figure 28: NASA Power Curve.

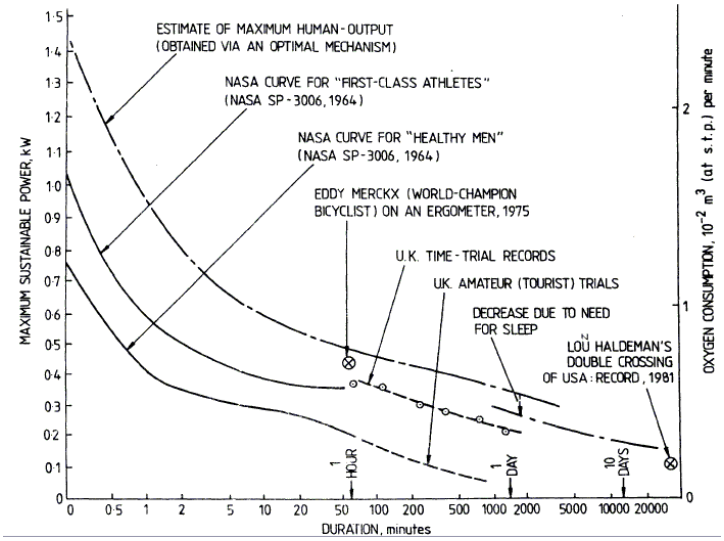

Figure 28: NASA Power Curve [15]

We used a load cell to measure the torque and an optical tachometer to measure the angular velocity at the dynamometer input shaft. The resistance of the dynamometer was changed by controlled by two variable resistor boxes. The data was collected using an Agilent data acquisition system so we could get real time power output feedback for the rider. This can all be seen below in Figure 29.

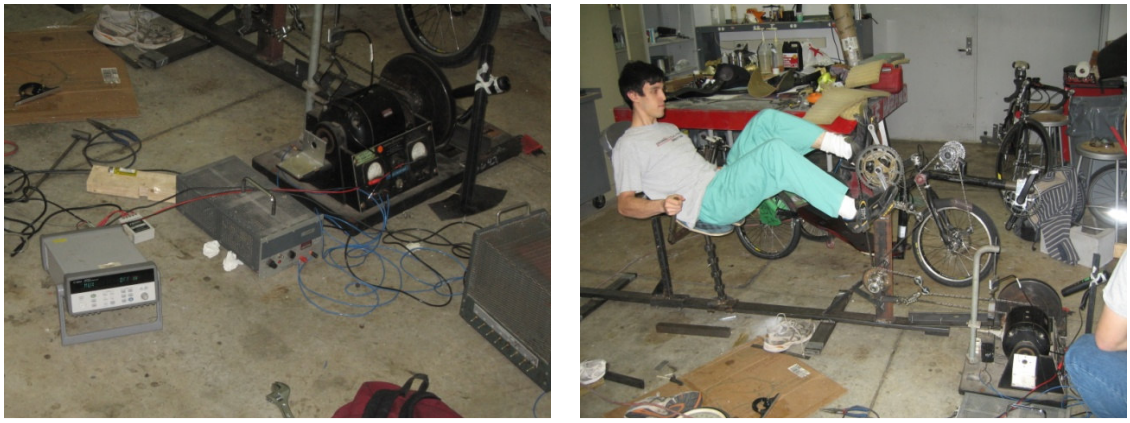

Figure 29: Power Chair

After preliminary testing to determine the appropriate test duration, a test of 2.5 minutes was chosen because the rider would be pushed beyond aerobic exercise into the anaerobic stage but not so far as to prevent recovery after a short period of recuperation. A 10 minute rotation was enacted with a 2.5 minute test, a 2 minute cool down, a 3.5 minute rest and stretch, and a 2 minute warm up then starting the cycle again. A range for the test variables was determined based on the expected dimensions of our vehicle from our preliminary aero analysis. We decided to perform a response surface design analysis on the data with a three by three matrix of test points. This would give us enough data points to produce a quadratic surface with a few extra degrees of freedom in case of outliers. The test variables and their corresponding design surface test values are shown in Table 8: Test Variable Ranges, these were necessary for the data analysis program to properly perform the analysis.

Table 8: Test Variable Ranges

Seat Angle (degrees)	Test Variable 'A'	Seat Height (in)	Test Variable 'B'
23	-1	-14.25	-1
36.5	0	-12	0
50	1	-9.75	1

The raw data from the data logger was compiled in Excel where the average power output over the duration of the test was determined. Also, after each test, the rider was asked to give a quality score of their impression of that test's configuration with a 1 being the best and a 10 being the worst. These values were then imported to Minitab 15 for analysis. Three riders were chosen for the test. All of the data points for the test were collected except for two points for the third rider, due to faulty equipment. Figure 30 shows the response surface for rider 1 using the average power.

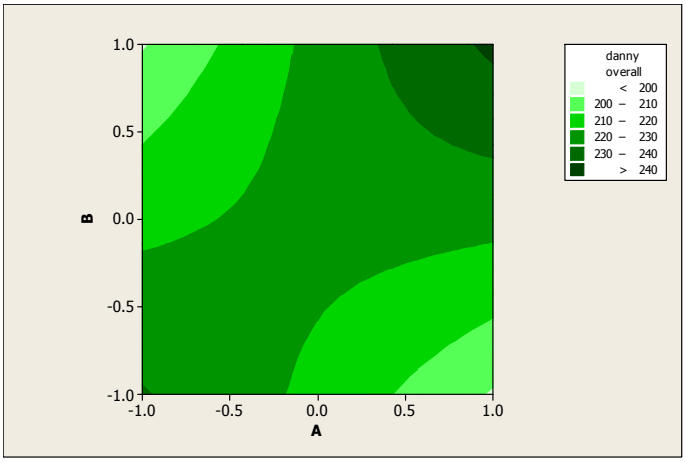

Figure 30: Rider 1 Overall Surface Plot

The lighter green zones in the corners represent the low power output locations while the dark green in the upper right corner shows that there is a maximum in that direction, but it appeared to be outside the bounds of our test range. In order

to make sure all of the data points were valid, a deleted t residual analysis was performed. This indicated that two of our points were outliers. After removing them, the surface plot was again generated, resulting in Figure 31.

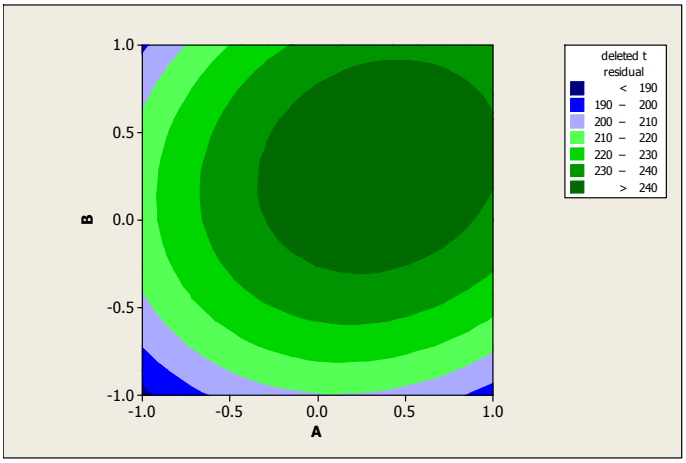

Figure 31: Rider 1 Overall with Outliers Removed

This brought the maximum power output to a location within our test range. The results were very similar with riders 2 and 3. After removal of the outliers, the maximum power output range was within our testing boundaries. The data from the three riders were then combined as three trials of the same test. The data was then filtered again for outliers and there were none. The results of the subjective opinion of the rider matched the power data well. The final response surfaces, after the outliers were removed, for all the riders combined are shown in Figure 32.

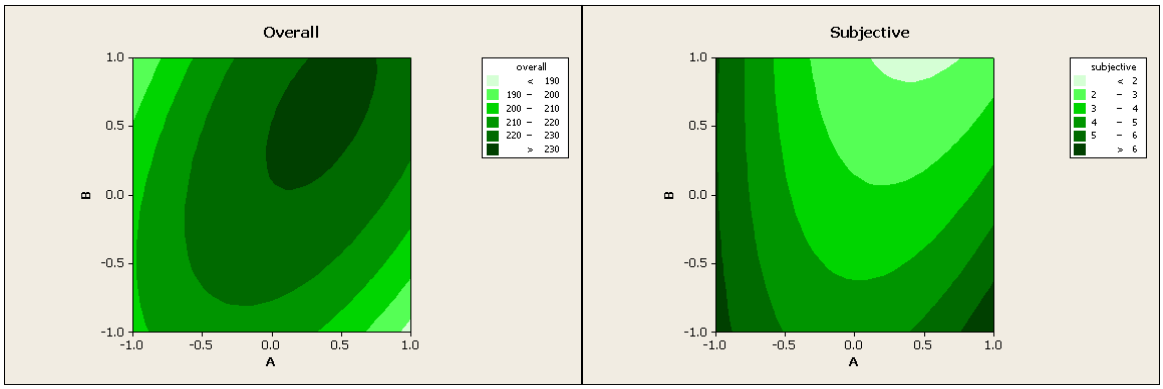

Figure 32: Combined Results

The maximum value was found for the combined overall response surface. The result that the test variable ‘A’ should be at a value of 0.3737 and the test value ‘B’ should be at a value of 0.6364 for the maximum power output. The optimizer results are shown in Figure 33 with the optimal values in red in brackets at the top.

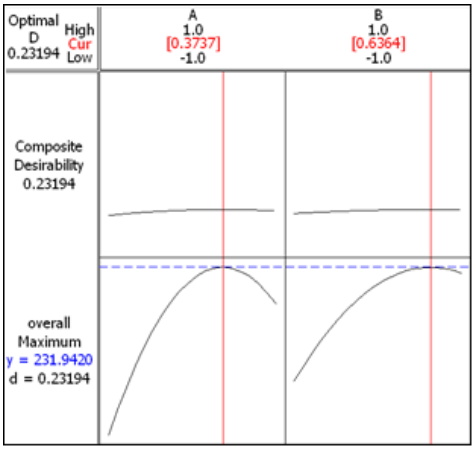

Figure 33: Optimizer Results

The test values had to then be converted to seat angle and seat height. Using the linear relationship between these and the test variables, the optimal seat angle was determined to be 42 degrees from horizontal and the optimal seat height from the bottom bracket was found to be -10.5 inches.

3.7 Chain Efficiency

In human powered competition small differences in weight and efficiency that may not even be tactilely perceivable can give an important edge to a team. Cost is a significant constraint for our club, and maintaining a proper budget is as important as assuring quality. To make sure that funds were not being improperly spent we designed a test to compare the efficiency of what is considered high quality bicycle chain to a less expensive competitor.

In order to test the efficiency of the chains we created an apparatus that tests how quickly a flywheel decelerates. A cassette was mounted to the flywheel and linked via a chain to a spring tensioned sprocket. Using an optical tachometer and data logger we recorded the deceleration between 1000 and 200 rpm. To increase the scope of our testing we added or removed lubricants and rusted one of the chains.

There was little difference within the same type of chain regarding whether or not it was lubricated. There was a more significant difference between the nine speed chain and the less expensive single speed chain. The nine speed chain was more efficient than the single speed chain. The rusted chain performed worst, as expected. It is then seen that chain lubrication is more important in preventing rust than actually directly improving performance during early stages of use. These tests justify the cost of buying higher performance chain for our vehicles and keeping them properly lubricated.

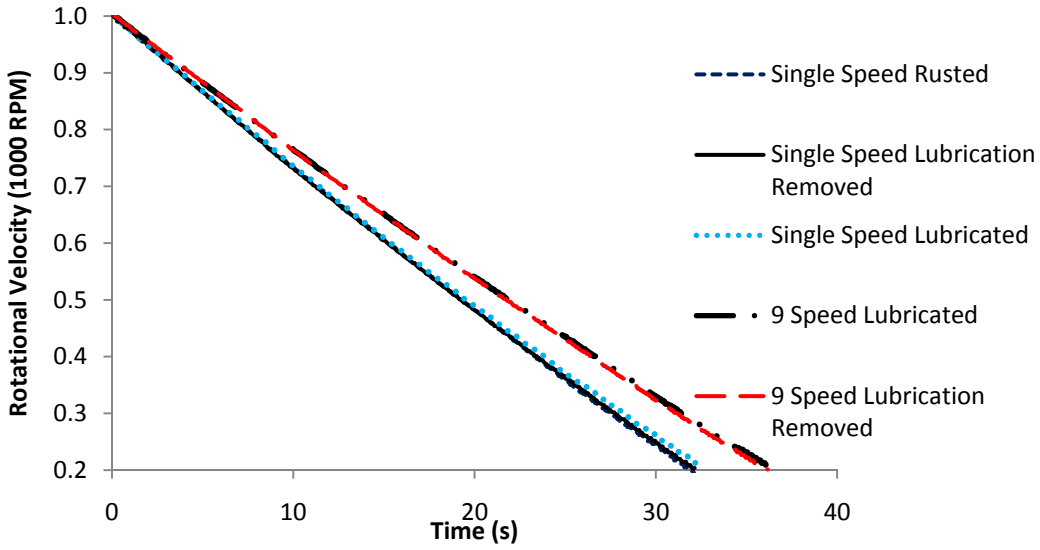

Figure 34: Rundown Time for Chain Efficiency Systems

4 Safety

Safety hazards can appear in the form of limited visibility, limited communication, fairing material choice, and the possibility for accidents. The safety of our riders was a top concern while designing the Mark IV and consequently no corners were cut to achieve this during cost and weight reduction steps. The strength, wear resistance, and integrity of the fairing and frame were previously addressed in the Design, Analysis, and Testing sections of this report. In order to increase the safety of the Mark IV compared to previous vehicles, design improvements were made to increase the field of view of the rider, prevent injury from carbon shards during a collision, and increase team communication. It is important to note that a commercially produced 4-point racing harness is used to firmly secure the rider inside the Mark IV in the event of a collision.

4.1 Field of View

The rider of the Mark IV can only avoid collisions and potential hazards if he/she is aware of them. In order to increase the riders' knowledge of the obstacles and vehicles around him/her it was necessary to develop a better field of view than in the vehicles of years past. Two steps were taken to improve this. The windshield was shaped so it yields a larger frontal field of view for the rider and mirrors were integrated into the design of the fairing so the rider can see behind himself/herself. The 2008 entry, the Infinity, had a field of view of 170 degrees in front of the rider. The Mark IV has a field of view of 190 degrees without the mirrors and with the mirrors its field of view increases to 320 degrees. Figure 35 compares the fields of view of the Infinity and Mark IV. The solid red arch represents the 190 degree blind spot of the Infinity and the solid blue arch represents the 35 degree blind spot of the Mark IV. This greatly improved field of view allows the rider a much better view of the vehicles around him/her, without the need to rotate their head.

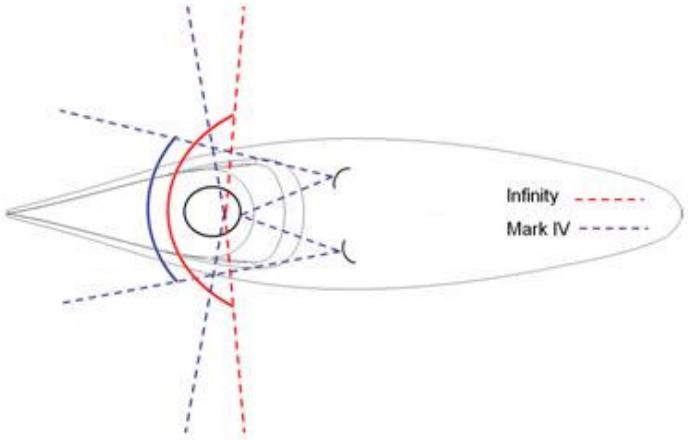

Figure 35: Mark IV vs. Infinity field of view

4.2 Carbon Shard Testing

The purpose of the carbon shard impediment tests is to determine if carbon fiber shards will penetrate a layer of Kevlar cloth during a composite failure. According to Human Powered Race America (HPRA), it is significantly safer to ride a Kevlar lined streamliner. In the event of a collision, the soft and net-like properties of the Kevlar will stop the razor-like carbon shards from breaking through and injuring the rider. Our goal is to determine if the Kevlar lining impedes carbon shard at all, and if so, we wish to see if any certain density of commonly available Kevlar cloth is needed to achieve this. In order to obtain definitive results we wanted to simulate the worst case scenario for carbon shard break through. To achieve this we laid up six 4x10 in samples. Each sample had three layers of 11oz 2x2 in Twill 6K tow 0.017 in thick carbon cloth covered with one layer of Kevlar. There were two samples of each of the following types of Kevlar: 5oz 4 Harness Satin 1140 tow 0.010 in thick weave, 5 oz 4 Harness Satin 1140 tow 0.010 in thick tape, and 1.7 oz plain weave 195 T965 tow 0.004 in thick weave. The samples were laid up in a medium cure room temperature epoxy and vacuumed bagged to emulate the actual vehicle fairing. After the six samples cured they were subjected to testing.

To simulate the worst crash situation possible the samples were broken over a square edge. Each sample was clamped between a flat plate of steel and the edge of a table. Then a downward impulsive force was applied to the overhanging part of the sample. Due to the qualitative nature of these tests, visual inspection is the primary judge of material success or failure. A description and a score of 1-10 are given to the sample to indicate the amount of shards and subsequently, danger to the rider. A score of 10 indicates a very safe break and a score of 1 indicates a razor-like edge.

The carbon control samples produced a significant amount of carbon shards and protruding fragments (Figure 36). The orange ovals signify areas with sharp carbon fiber spikes jutting out. The yellow circles signify areas where the carbon has become discontinuous and there is a flat carbon edge exposed. Because of the significant amount of sharp carbon exposed edges and protruding shards, the carbon control samples get a safety score of 2.

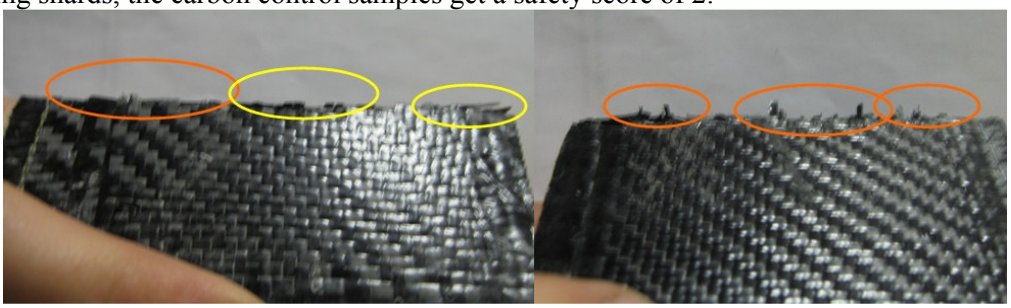

Figure 36: Exposed Carbon Shards

When compared to the carbon control the 1.7oz or thin Kevlar showed significantly less carbon shards protruding through the surface (again the orange circle in Figure 37). The Kevlar fabric was torn across most of the sample though, so even though it retained the shards very well it did not stop the exposure of the carbon fiber (yellow circles) when bent to the 90 degrees. Due to the minor amount of protruding carbon shards, but still significant amount of exposed carbon the thin Kevlar gets a safety score of 5.

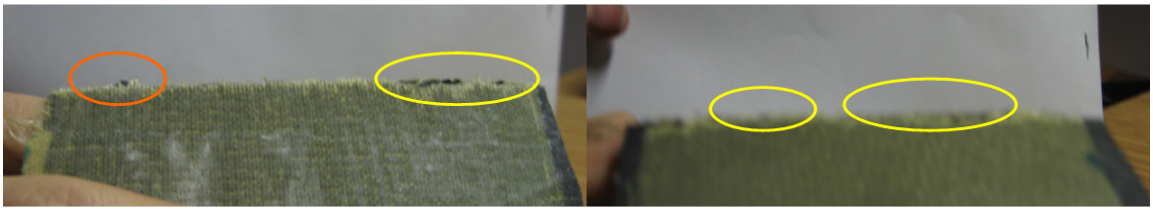

Figure 37: Thin Kevlar

When compared to the carbon control and the thin Kevlar the 5oz Kevlar weave showed significantly less exposed carbon (yellow circles in Figure 38: 5oz Weave) and almost no carbon fibers protruding from the surface. This step up in protection from the thin Kevlar warrants a safety rating of 7 for the 5 oz weave.

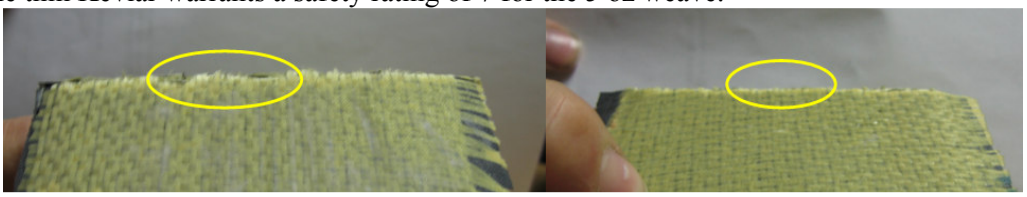

Figure 38: 5oz Weave

When compared to the 5oz Kevlar weave the 5oz Kevlar tape exhibited nearly the exact same results. There was little exposed carbon (yellow circles in Figure 39) and almost no carbon fibers protruding from the surface. The 5oz tape is just as good at protecting the rider as the 5oz weave so it earned a safety rating of 7.

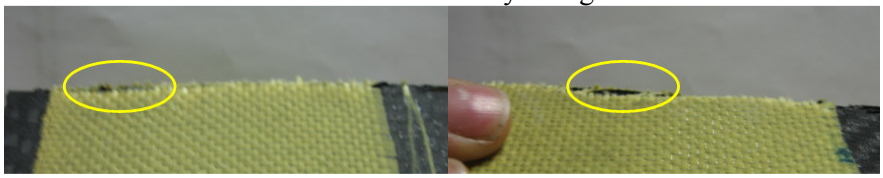

Figure 39: 5oz tape

Comparing the safety scores of the 3 different types of Kevlar fabrics and the carbon control yields the following data (Table 9).

Table 9: Kevlar safety scores

Sample	Carbon Control	Thin Kevlar	5oz Kevlar weave	5oz Kevlar tape
Score	2	5	7	7

The carbon sampled scored the lowest with a safety score of 2 out of 10. The thin 1.7 oz Kevlar came in 3rd place with a safety score of 5 out of 10 and the 5 oz Kevlar tape and weave both performed the same and earned a safety score of 7 out of 10. From these results we confirmed that there is a significant safety improvement from the straight carbon to the Kevlar covered carbon. Then there is still further improvement in safety when a higher density Kevlar is used. Because of these results we are going to utilize the 5 oz Kevlar weave for our vehicle fairing.

4.3 Communication

Improving team communication greatly increases the safety of the rider. Hazards that may not be apparent to the rider in the HPVC endurance race can be relayed by spotters stationed around the course. Using radios, the rider, pit crew, and spotters can communicate instantaneously. The team can respond within seconds of a crash or equipment failure on the course. In addition, radio communication is invaluable for race strategy, rider performance, and pitting strategy.

4.4 Seatbelt Testing

For the Mark IV, it was decided that a 4-point harness would provide the greatest strength and be the safest type of seat belt for the riders. A 4-point harness intended for automotive racing was purchased for use in the Mark IV. To test the 4-point harness attachment, the seat belt was riveted into a test roll cage using holding plates made of aluminum and five steel rivets for each attachment point. Only the top two mounts were added for testing purposes. After building a mounting rig to hold the roll cage in place, a load was applied to the belt mounts. After a load of 1106 lb_f was reached, one rivet gave way, but the others held. However, in the final vehicle, all four ends on the harness will be secured.

5 Conclusions

Our mission statement this year was: "Design, Test, Build and Race the Mark IV, a safe vehicle with improved endurance performance and a top speed exceeding 45mph in competition." To do this we have done significant analysis and testing as part of the design process. We tested the relationship between ergonomics and power output, and used FloWorks to test different aerodynamic shapes to increase our sprint speed. We determined the optimum steering geometry to increase our stability for endurance. We decided to implement a ribbed tub frame rather than a monocoque frame in order to reduce the weight. We performed significant materials testing to determine the best strength to cost ratio and strongest ribbing method. All of these, and the improvements we have made in the areas of safety, culminate in the safe and reliable human powered vehicle we have named the Mark IV.

Appendix 1 Costs

Fabrication		
Vehicle Parts	585.90	
Composite Materials	1,810.95	
	Total	Unit Cost
	2,396.85	2,396.85

Equipment		
Milling Machine	4,000.00	
Table Disk Grinder	100.00	
Lathe	3,000.00	
Vertical Band Saw	1,150.00	
Welding Machine	2,100.00	
Plug Construction	700	
	Total	Unit Cost
	11,050.00	15.35

Overhead		
Building Rent	3,000	
Utilities	1,000	
Advertising	1,000	
	Total	Unit Cost
	5,000	41.67

Employees	Qty[16]	Hourly	Yearly
Floor workers	5	14.59	30,347.20
Welder	1	40.83	84,916.00
Machinists	2	43.73	90,948.00
Engineer	1	-	130,000.00
	Total	Unit Cost	
	336,211.20	2,801.76	

Total Vehicles	Total Unit Price
720	5,255.62

Total Return	Sale Price
756,809.84	6,306.75

References

[1] Shenoi, R. A. and Wellicome, J.F., 1993, *Composite Materials in Maritime Structures*, Cambridge University Press, Cambridge, Great Britain

[2] Cornelius, C.J., 1990, "Rear Steering Recumbent Bicycles," *Human Power,* D.G. Wilson, Indianapolis, Vol. 8 # 2, pp 6,7.

[3] Whitehead, J., 1990, "Rear Wheel Steering Basics," *Human Power,* D.G Wilson, Indianapolis, Vol. 8 #4, pp 9-14.

[4] Kyle, C. and Berto, F., 2001. "The Mechanical Efficiency of Bicycle Derailleur and Hub-Gear Transmissions," *Human Power ,* D.G Wilson, Indianapolis, No. 52, pp 3-11.

[5] Roberts, T. M., Goff, Z.H., et al., 2008, *2008 HPVC Single Rider Entry Team 35 Design Report*, Rose-Hulman Institute of Technology, Terre Haute, IN

[6] Patterson, W. B., 2004, *The Lords of the Chainring* Santa Maria.

[7] Le Hénaff, Y., 1987, "Dynamical Stability of the Bicycle," *Human Power,* D.G Wilson, Indianapolis, Vol. 6 #1, pp 15-17.

[8] Papadopoulos, J. and Ruina, A., 1987, "Discussion of Le Hénaff's Paper," *Human Power,* D.G Wilson, Indianapolis, Vol. 6 #1pp 18,19.

[9] Five, M., 2003, "An Introduction to Bicycle Geometry and Handling," http://www.dclxvi.org/chunk/tech/trail/, Accessed 2/21/2009.

[10] Putnam, J., "Steering Geometry: What is Trail," http://www.phred.org/~josh/bike/trail.html Accessed 2/21/2009.

[11] Riley, W. F., Sturges, L. D., and Morris, D. H., 2002, *Statics and Mechanics of Materials: An Integrated Approach*, John Wiley & Sons Inc., New York.

[12] ANSYS, Inc, "Bearing Load" *Release 11.0 Documentation for ANSYS Workbench.*

[13] Hed, Steve, 01/21/2009, *Telephone Interview.*

[14] Brunner, T., "The development of 'The World's Fastest Bicycle,' Lightning X-2," *Human Power,* D.G Wilson, Indianapolis, Vol. 3 #1, 1984 pg 21-22.

[15] Whitt, F. R., and Wilson, D., 1982, *Bicycling Science, 2nd Edition*, The MIT Press, 1982, Boston.

[16] Bralla, J.G., 1998, *Design for Manufacturability*, McGraw-Hill, New York.